Progress In Electromagnetics Research C, Vol. 127, 71–82, 2022

A Dual Adaptive Inertia and Damping Control Strategy of ANFIS-VSG for Direct-Drive Permanent Magnet Synchronous Wind Generator Systems

Yang Zhang[1], Anping Chen[1], Jiangwei Deng[1], Yihan Liu[1], Sicheng Li[1], and Zhun Cheng[2, *]

Abstract—In the conventional virtual synchronous generator (VSG) dual adaptive inertia and damping control schemes, the inertia J and damping D exhibit different variation patterns in different time intervals and are mutually constrained. To address this problem, an adaptive neural-fuzzy network inference system (ANFIS)-based dual adaptive inertia and damping VSG control technique applied to the direct-drive permanent magnet synchronous wind generator (D-PMSWG) system is proposed in this paper. In ANFIS-VSG, the controller is designed on the basis of the ANFIS control principle, and the input and output data are collected by PID control. The Sugeno-type ANFIS controller model is adopted to train the fuzzy inference system (FIS) online. Moreover, the virtual inertia and damping coefficients can be dynamically adjusted in real time according to the frequency variation without taking the different variations and mutual constraints of inertia J and damping D in different intervals into consideration, so the design difficulty and calculation process can be simplified, and the accuracy of the proposed control algorithm is enhanced through training. Furthermore, when the system is subject to load changes, integrating into the grid from an islanded state, and when the output power sets value steps, the power-frequency characteristics and the anti-interference capability of the three-phase output current of VSG can be improved. Finally, the proposed control strategy is simulated and analyzed based on Matlab/Simulink simulation software, which proves the correctness and effectiveness of the proposed control algorithm.

1. INTRODUCTION

D-PMSWG system is widely employed because it removes deteriorating parts like gearboxes, considerably reduces maintenance costs, and provides a reliable fault ride-through capability [1, 2]. Permanent magnet synchronous generators (PMSGs) significantly contribute to the stability of power systems with their inherent damping and inertia [3], and have been considered a promising solution to high power wind turbine applications [4–6]. However, with the increasing penetration of wind power, the wind power system is connected to the grid via a power electronic inverter interface, which prevents the power system's functioning from being supported by inertia and damping. Since VSG technology enables grid-connected inverters to simulate the operation mechanism of synchronous generators, the inverters produce inertia and damping similar to those of synchronous generators, which can increase the anti-interference capability of grid-connected inverters, enhance the stability of the power system, and provide certain voltage and frequency support to the grid [7]. Thus, this control mechanism is presently gaining a lot of attention from academics and is typically utilized in the production of new energy [8].

Received 3 October 2022, Accepted 16 November 2022, Scheduled 28 November 2022

* Corresponding author: Zhun Cheng (120277982@qq.com).

[1] Hunan University of Technology, Zhuzhou 412007, China. [2] Hunan Railway Professional Technology College, Zhuzhou 412001, China.

Even though grid-connected inverters with VSG control strategies may possess the external characteristics and rotor inertia characteristics similar to those of synchronous generators, the majority of the studies that are currently available for conventional virtual synchronous machine control strategies use a fixed and constant rotational inertia, which cannot take into account rapidity while ensuring system stability. In practice, the virtual inertia of the inverter can be adaptively selected to a more suitable value depending on the actual application. Hence, a VSG control algorithm with adaptive virtual inertia has been proposed in [9–11], taking not only the output power angle curve and the physiological significance of synchronous generator rotor inertia, but also the deviation and rate of change of angular velocity into consideration, and the fluctuation of system frequency can be adjusted immediately and suppressed effectively when the system is exposed to load disturbance. In [12, 13], for doubly-fed wind power systems, the variation range of the virtual inertia control parameters of the wind turbine was rectified based on the relationship between the differential coefficients of the wind turbine auxiliary inertia control and the equivalent inertia constant of the wind turbine. The anti-interference capability and the dynamic stability of the system in frequency were improved by constructing the correlation between the rate of change of frequency and the virtual inertia. Based on the aforementioned work, an interleaved adaptive virtual synchronization control strategy for doubly-fed wind turbines is proposed in the literature [14], considering the variation threshold of the output active power of doubly-fed wind turbines.

However, the effects of damping coefficients are routinely neglected in the majority of studies on VSG adaptive control. To cope with this problem, a virtual inertia fuzzy adaptive control method for wind turbines based on frequency response interval division is proposed in [15] to accelerate the system frequency recovery while the damping frequency changes rapidly. In [16, 17], to ensure the stability of the parameters in adaptive tuning by limiting the system to an underdamped condition, the functions related to D and J were determined under the condition of taking into account the damping ratio of the system and adjusting J according to the rate of change of the frequency. In [18–21], the trends of J and D at various stages of power regulation are taken into account. That is, the damping coefficient D is adjusted according to the VSG's angular velocity deviation to reduce the system's frequency deviation, and the inertia J is changed according to the rate of change of the angular velocity deviation, improving the system's dynamic performance without compromising the stability of the system.

Yet the traditional adaptive inertia and damping control strategy of VSG requires consideration of the variation of J and D in different intervals, which increases the complexity of the system, and the above control methods are prone to integral saturation when being subjected to multiple perturbations and cannot meet the demand of fast frequency response [22, 23]. To cope with this problem, an ANFIS-VSG inertia-damping dual adaptive control strategy for D-PMSWG systems is proposed in this paper. Firstly, by analysing the frequency variation pattern corresponding to inertia and damping, the controller is designed based on the ANFIS control principle. In the controller design, the selection of control variables, and affiliation functions, the acquisition of input and output data using PID control, the correction of the affiliation function parameters according to the selected error criterion, and the training of the fuzzy inference system (FIS) model using a Sugeno-type ANFIS controller are all introduced. Furthermore, the strategy does not need to consider the different changes and mutual constraints of inertia J and damping D in different intervals. Compared with the typical VSG inertia-damping dual adaptive control strategy, the frequency response characteristics during load changes and islanding are getting better, the ability for output active power to track the trajectory of the given value is optimized. By the way, the VSG three-phase output current transition is smoother, and the algorithm error is significantly reduced when the above operating conditions of the system vary.

2. DUAL ADAPTIVE INERTIA AND DAMPING CONTROL THEORY OF ANFIS-VSG

2.1. Variable Properties of Virtual Inertia and Virtual Damping

In the conventional dual adaptive inertial and damping VSG control, the rate of change of angular velocity ω is determined by the inertia, and the amount of change of ω is determined by the damping, both of which affect the change of active power. When the value of J is chosen too small, although the system response time is reduced, and the power oscillations may not be suppressed due to the lack

of inertial characteristics. However, when the value of J is chosen too large, even though the power oscillations can be efficiently restrained, the system frequency response time has increased. Similarly, the selection of virtual damping factor D also affects the performance of power oscillation suppression.

The VSG power angle curves shown in Fig. 1 have different principles for the selection of inertia and damping under different conditions corresponding to the four operating intervals. The selection principles are presented in Table 1.

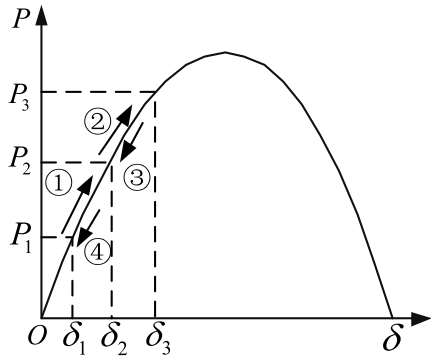

Figure 1. Power-angle curve of VSG.

Table 1. Selecting principle of J and D under different conditions.

Interval	$\Delta\omega$	$\mathrm{d}\omega/\mathrm{d}t$	$\Delta\omega\mathrm{d}\omega/\mathrm{d}t$	The change of J	The change of D
①	>0	>0	>0	increase	Increase appropriately
②	>0	<0	<0	decrease	Increase appropriately
③	<0	<0	>0	increase	Increase appropriately
④	<0	>0	<0	decrease	Increase appropriately

However, since ANFIS integrates the self-learning capability of neural network with the fuzzy inference capability of fuzzy control, there is no need to take the mutual constraint of inertia J and damping D into account and to design the affiliation function artificially. Based on the data gathered by PID, the variation law of J and D can be learned, and the resulting Sugeno-type fuzzy inference system may be used as the reference model for VSG inertia and damping adaptive control. Moreover, the ANFIS controller provides real-time output of inertia and damping deviations to adjust frequency deviations during VSG load throwing and cutting online, while reducing active power deviations.

2.2. Mathematical Model and Control Principle of the Dual Adaptive Inertia and Damping Control of ANFIS-VSG

The essence of VSG is to simulate the principle of operation of a synchronous generator by controlling the inverter, thereby obtaining the inertia characteristics and damping characteristics similar to those of a synchronous generator, and improving the immunity of the system frequency and output active power.

In order to specifically depict the operating characteristics of synchronous generators in a variety of applications, various mathematical models such as second-order and third-order have been proposed by scholars. In purpose to reflect the inverter operating characteristics of VSG control and to avoid the complex electromagnetic coupling relationship and output power decoupling process of synchronous generators, the VSG model is constructed using the second-order model. The rotor equations of motion and the stator electrical equations of VSG are expressed as

$$\begin{cases} P_m - P_e - D\left(\omega - \omega_m\right) = J\omega d\left(\omega - \omega_m\right)/dt \\ E = E_0 - I\left(R_i + jX_t\right) \end{cases} \tag{1}$$

where P_e is the stator virtual electromagnetic power, which is replaced by the inverter output active power, considering the small equivalent output resistance of the inverter main circuit and the simplification of power calculation; both D and J can be developed flexibly in accordance with the control requirements and are not constrained by the mechanical properties of synchronous generators; E, E_0, and I represent the stator winding terminal voltage, stator winding induced electric potential, and stator current of the synchronous generator, respectively; R_i is the filtering resistance, equivalent to the stator armature resistance; X_i is the filter reactance and equated to the synchronous reactance.

The control block diagram of the proposed ANFIS algorithm-based dual adaptive inertia and damping control strategy is given in Fig. 2.

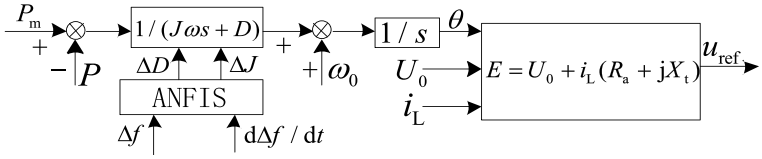

Figure 2. Block diagram of VSG dual adaptive inertia and damping control based on ANFIS.

The core idea of the dual adaptive inertia and damping control of VSG based on ANFIS algorithm is to regulate the values of VSG rotational inertia and damping in real time by ANFIS algorithm and consequently optimize the power and frequency adjustment performance of the control system. The basic control block diagram of the improved method applied to the grid-connected inverter of the D-PMSWG system is shown in Fig. 3. In Fig. 3, four main modules are composed: virtual governor, virtual exciter, ANFIS-based VSG dual adaptive inertia and damping control algorithm, and voltage and current dual loop; PCC indicates the common coupling point.

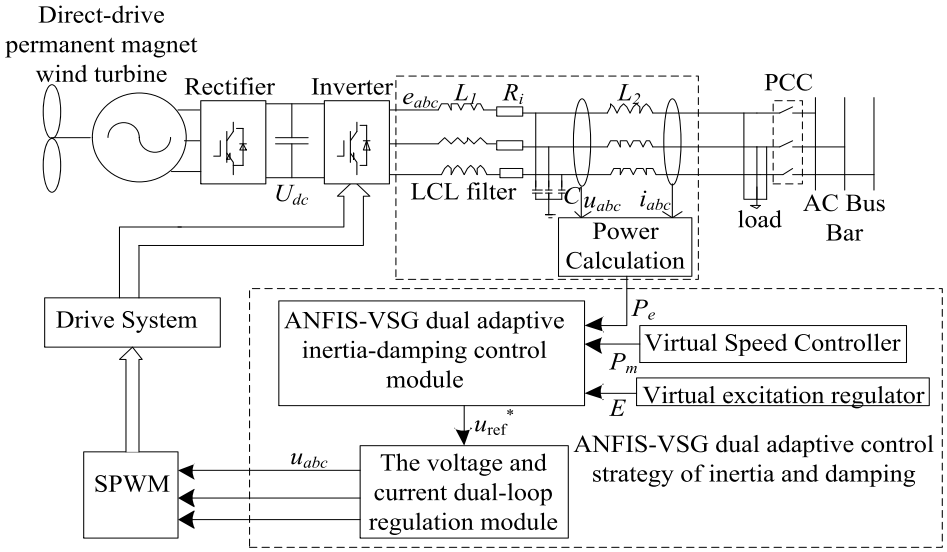

Figure 3. Block diagram of dual adaptive inertia and damping VSG control in DPMSWG system.

As shown in Fig. 3, e_{abc}, u_{abc}, and i_{abc} are the equivalents of the induced electromotive force, output voltage, and grid current of the synchronous generator, respectively. u_{abc} and i_{abc} are substituted into Equations (2)–(3) after Park transformation to obtain the output active power P and reactive power Q from the grid-connected inverter. The virtual speed controller realizes the modulation of the inverter output active power and provides the virtual mechanical power P_m signal for the VSG virtual inertia adaptive algorithm. The virtual excitation regulator is for the stabilization of inverter output voltage and regulation of reactive power balance. The ANFIS-VSG dual adaptive inertia-damping control module is for simulating the characteristics of parallel synchronous generator operation and adjusting

inertia and damping in real time. The voltage and current dual-loop regulation module enables a rapid response of the inverter output voltage and accurate tracking of the commanded voltage. The sine pulse width modulation (SPWM) module generates a pulse width modulation (PWM) signal from the reference voltage, which is generated by the voltage and current dual-loop regulation module and drives the IGBT to finalize the three-phase electrical output.

$$P = \frac{3}{2(\tau s + 1)}(e_{oq} i_{oq} + e_{od} i_{od}) \tag{2}$$

$$Q = \frac{3}{2(\tau s + 1)}(e_{oq} i_{oq} - e_{od} i_{od}) \tag{3}$$

3. ANFIS CONTROLLER DESIGN

3.1. ANFIS Controller Construction

The ANFIS has combined fuzzy systems with neural networks, taking full account of the complementary nature of each and has shown excellent results in handling large-scale fuzzy application problems [24, 25]. The ANFIS is a hybrid learning algorithm to locate the corresponding mapping relationship between input and output data to ascertain the optimal assignment of the affiliation function, and it is therefore possible to obtain a system model by the ANFIS method. The ANFIS tunes the Sugeno-type fuzzy controller by means of a neural network, adopting either a separate back-propagation algorithm or a combination of this algorithm with the least squares method to accomplish the tuning of the system affiliation function parameters. Further, the ANFIS controller is structured like a neural network and functions as a fuzzy system, as demonstrated in Fig. 4. In Fig. 4, the inputs are represented by x_1 and x_2; the degree of rule usage is denoted by w_1 and w_2; the linguistic variables are represented by A_1, A_2, B_1, and B_2; the results of the normalized calculations are specified by $\bar{w}_1$ and $\bar{w}_2$; nodal functions stated as $\bar{w}_1 y_1$ and $\bar{w}_2 y_2$; the output quantity is designated by y.

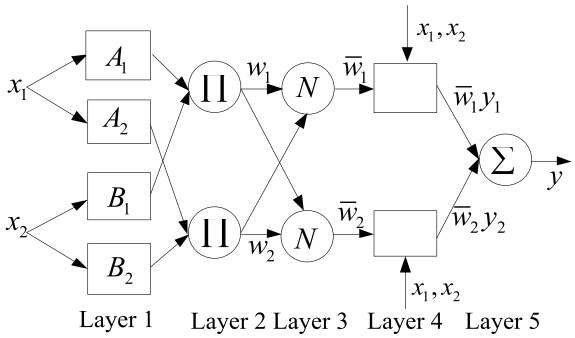

Figure 4. Structure diagram of ANFIS.

Layer 1: Each node i in this layer is an adaptive node, and the output of each node is the degree of the affiliation function of the input function, and the input data in this paper are the frequency deviation Δf and the derivative of the frequency deviation $\mathrm{d}\Delta f/\mathrm{d}t$.

$$\begin{cases} O_{1,i} = \mu_{Ai}(x_1), & i = 1, 2 \\ O_{1,i} = \mu_{Bi}(x_2), & i = 3, 4 \end{cases} \tag{4}$$

If the affiliation function is a bell-shaped function, then:

$$\mu_x = \frac{1}{1 + \left| \dfrac{x - c}{a} \right|^{2b}} \tag{5}$$

where $\{a, b, c\}$ is the parameter setting; x_1 and x_2 are the input values; $O_{1,i}$ is the degree of affiliation function; μ_{Ai} and μ_{Bi} are the affiliation functions of linguistic variables A and B, respectively; μ_x is the general affiliation function.

Layer 2: The outcome of this layer is the product of all the input signals, which is used to match the antecedents of the fuzzy rules and compute the usage degree for each of the rules.

$$O_{2,i} = w_i = \mu_{Ai}(X_1) \times \mu_{Bi}(X_2), \quad i = 1, 2 \tag{6}$$

Layer 3: Defuzzification layer for normalized computation.

$$O_{3,i} = \bar{w}_i = \frac{w_i}{w_1 + w_2}, \quad i = 1, 2 \tag{7}$$

Layer 4: Each node represents a node function.

$$O_{4,i} = \bar{w}_i y_i = \bar{w}_i(c_{i1}x_1 + c_{i2}x_2 + c_{i0}), \quad i = 1, 2 \tag{8}$$

In the formula, node parameter settings, rule usage, normalized calculated values, and node function settings are marked by $\{c_{i1}, c_{i2}, c_{i0}\}$, w_i, $\bar{w}_i$, and y_i, respectively.

Layer 5: The output layer is entirely defuzzified to achieve clarity calculation, and the common methods are average maximum affiliation method, median method, weighted average method, etc. In this paper, the weighted average method is utilized, and the output quantities are virtual inertia deviation ΔJ and virtual damping deviation ΔD.

$$O_{5,i} = \sum \bar{w}_i y_i = \frac{\sum\limits_i w_i y_i}{\sum\limits_i w_i}, \quad i = 1, 2 \tag{9}$$

3.2. Training Consequences of ANFIS

The system designed in this paper uses neural network for fuzzy control to automatically extract fuzzy rules and fuzzy affiliation function, as to make the overall system an adaptive fuzzy neural network system. The ANFIS automatically calculates the learned error from the actual output value of the system and the expected output value when studying, and automatically adjusts the system parameters through the error back propagation algorithm to fulfil the objective of minimizing the error. The adjusted system parameters mainly include weights, Gaussian function central and width.

The ANFIS trained in this paper is a first-order Sugeno model with 7 fuzzy subsets of inputs 1 and 2, and the subordinate functions are all Gaussian-type functions with an allowable tolerance of 0.005 and a training frequency of 500. The input figures comprise frequency deviation Δf and derivative of frequency deviation $\mathrm{d}\Delta f/\mathrm{d}t$, and the output data are virtual inertia deviation ΔJ and virtual damping deviation ΔD, which are obtained from the PID simulation control experiments. The input variable affiliation function of ANFIS is shown in Fig. 5, which can generate the corresponding fuzzy rules straightly after neural network training without referring to the inherent fuzzy control rule table.

The deblurring method adopted in this paper is the weighted average method. It is comparatively simpler to calculate than the commonly utilized median method. In this way, the effect of the most value affiliation point is weakened, and the clarification outcome is more accurate. Fig. 6(a) and Fig. 6(b) represent the adaptive neural network fuzzy inference control surface for J and D, respectively. It can be seen that the control surfaces of the virtual inertia variation ΔJ and virtual damping variation ΔD from the system outputs are smoother to achieve more effective control.

4. ANALYSIS OF SIMULATION RESULTS

In order to validate the correctness and feasibility of the proposed ANFIS-VSG dual adaptive inertia and damping control strategy, the ANFIS-VSG control model of the D-PMSWG system illustrated in Fig. 3 was established in the MATLAB/Simulink software environment, and the major parameters of the simulation are given in Table 2.

Case 1: The simulation is scheduled from 0.0 s to 0.5 s; the system is initially operated without load and in islanded mode; 15 kW of load is added at 0.2 s and integrated into the grid at 0.5 s. This procedure is investigated to study the frequency stability of the system under load change and switching

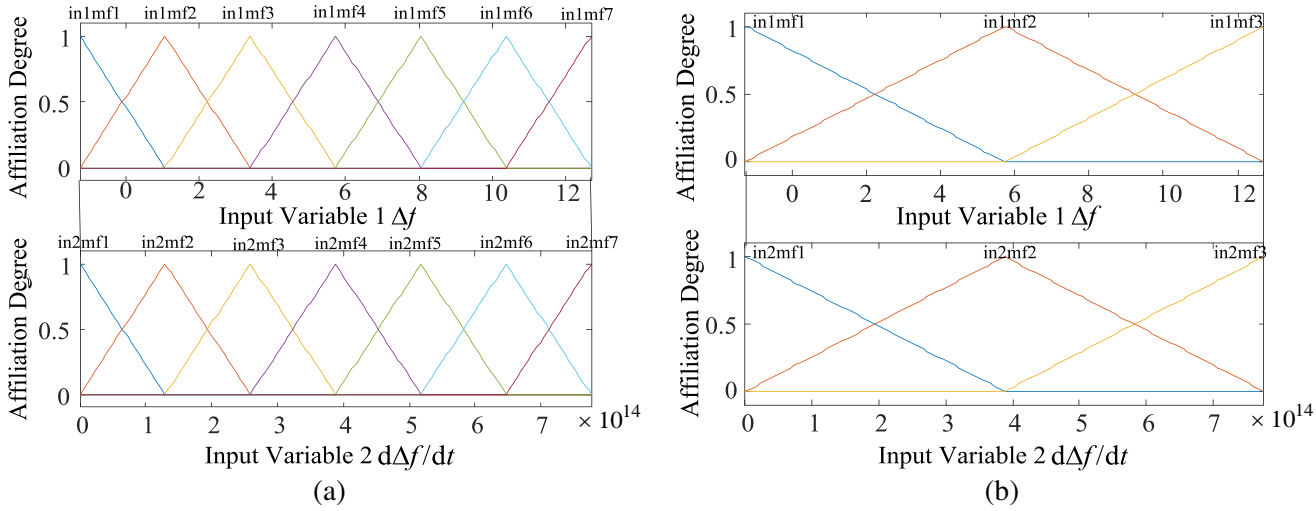

Figure 5. Membership function graph. (a) Adaptive input variables for J. (b) Adaptive input variables for D.

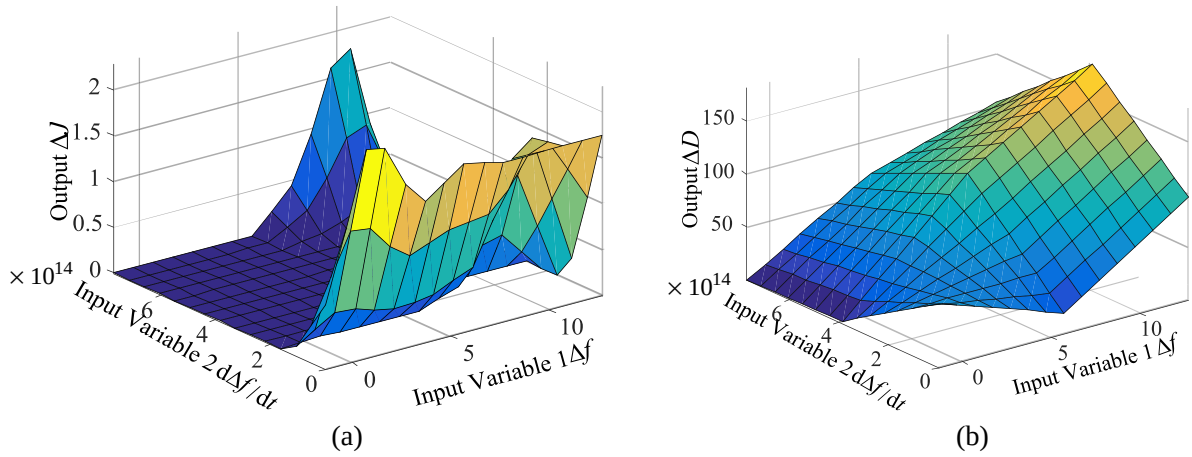

Figure 6. Neural network fuzzy inference control surface. (a) Adaptive neural network fuzzy inference control surface for J. (b) Adaptive neural network fuzzy inference control surface for D.

Table 2. Main parameters of simulation system.

Parameters	Values and Units
DC Voltage	700 V
Single-phase Line Voltage RMS	380 V
Filter Inductance Reactance	1 mH
Filter Internal Resistance	0.5 Ω
Filter Capacitor	40 μF
Nominal Angular Speed	314 rad/s
Frequency Deviation Feedback Coefficient	2000
Feedback Coefficient of P and Q Deviation	0.0005

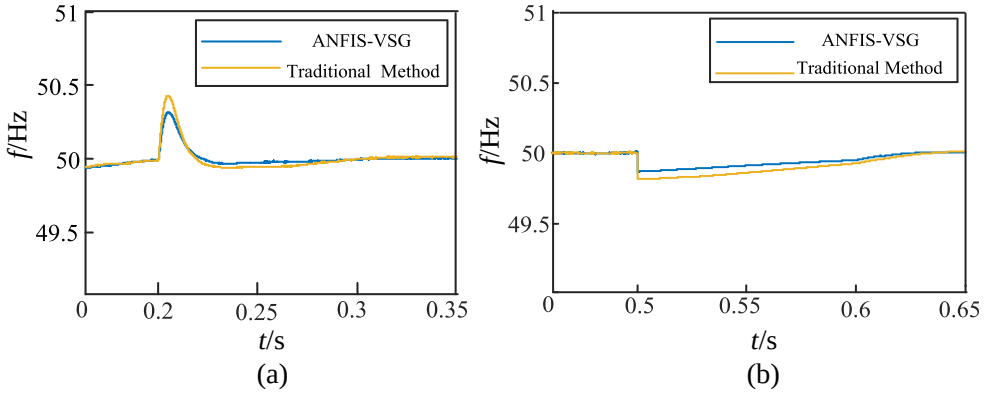

Figure 7. VSG output frequency change comparison diagram. (a) Frequency variation curve when the load increases in islanded operation mode. (b) Frequency variation curve for grid-connected from islanded operation mode.

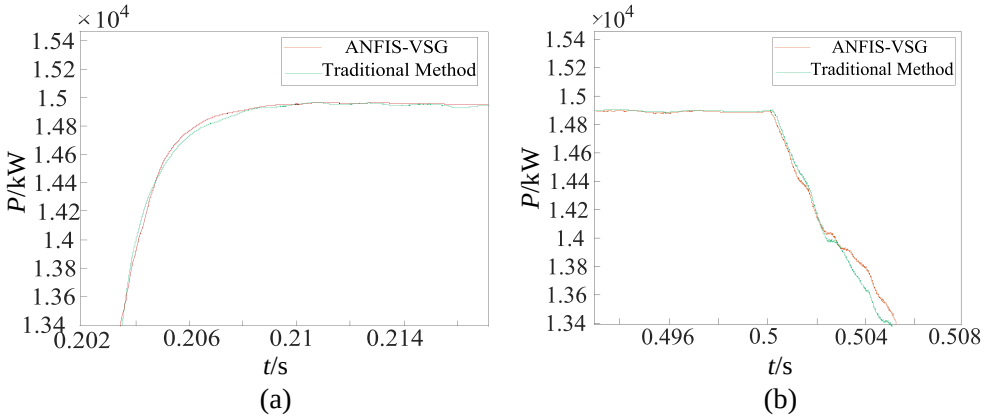

Figure 8. Comparison graphic for the active power change of the VSG output. (a) Output active power variation curve when the load increases in islanding operation mode. (b) Output active power variation curve when the system is connected to the grid from islanding mode.

from islanding mode to grid operation, and the comparison results of the proposed strategy with the conventional VSG dual adaptive inertia and damping method are depicted in Fig. 7.

Analysis of Fig. 7(a) revealed that the dynamic performance of the inverter control system with the ANFIS-VSG dual adaptive inertia and damping control strategy was optimized. The simulation throws in a large capacity load of 10 kW at 0.2 s when the system is in islanding operation mode, resulting in a frequency increase. Compared with the traditional method, the modified adaptive control strategy stabilizes the frequency at a faster rate and reverts to 50 Hz at 0.26 s, while the traditional method adjusts to 50 Hz at 0.29 s. Besides, the enhanced method limits the oscillation amplitude to a smaller extent, whose frequency oscillation amplitude is 0.11 Hz less than that of the traditional method, which effectively suppresses the interference brought by the large-capacity load to the system in a short period of time.

According to Fig. 7(b), when the system enters the grid-connected operation mode from the islanded operation mode at 0.5 s, the system frequency drops slightly, that is, the frequency of the improved method drops 0.11 Hz and returns to stability at 0.6 s, whereas the frequency of the traditional method drops 0.15 Hz and does not recover to stability until 0.63 s. It can be demonstrated that, by adopting the enhanced method, the frequency fluctuation is simultaneously reduced; the frequency response velocity is accelerated; and the anti-interference capability gets stronger when the system is connected to the grid in islanded operation mode.

As indicated in Fig. 8(a) and Fig. 8(b), the proposed strategy only balances the active power

at 0.2 s ahead of the conventional control method by 0.002 s when the system is put under load from islanding mode. While when the system is connected to the grid at 0.5 s, the VSG output active power of both methods decreases almost concurrently. Nonetheless the active power under the proposed control policy declines slightly less and picks up slightly faster. It can be concluded that the power-frequency characteristics of the proposed control strategy in islanding mode are faintly superior to those of the conventional method.

Case 2: The output active power reference value is set to 10 kW at 0.6 s, and the output active power given value is abruptly changed to −10 kW at 1 s. This process detects the dynamic tracking performance of the controller, and the simulation results compared with the conventional method are shown in Fig. 9.

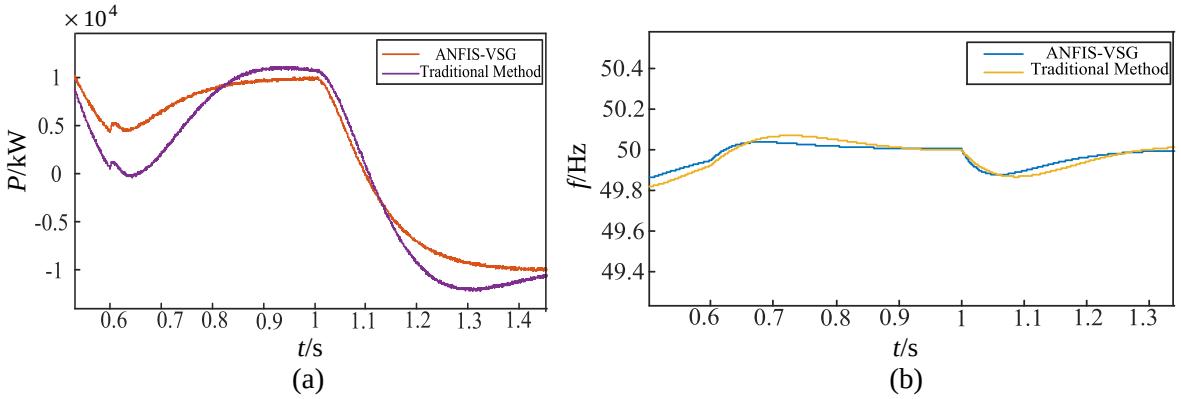

Figure 9. Comparison diagram of power frequency curve when the given value of active power changes. (a) The change curve of VSG output active power when the given value of active power is varied. (b) System frequency change curve when the given value of active power is varied.

As presented in Fig. 9(a), to confirm the dynamic tracking performance of the ANFIS controller, the reference active power is set to 10 kW at 0.6 s and −10 kW at 1 s. In Fig. 9(a), the error between the given and actual values of the proposed control strategy is less than 0.05 kW during the period of 0.6 s–1.45 s, while the error between the given and actual values of the conventional method is less than 1 kW. The results reveal that the improved approach provides better tracking of the given active power, higher control accuracy, and faster tracking speed.

By analysing Fig. 9(b), it can be detected that the system frequency is disturbed and changed when the output active set value is altered. At 0.6 s, the overshoot of the improved method is diminished by 0.06 Hz, and the response time is shortened by 55.26% with respect to the conventional method. At 1 s, the frequency overshoot of the improved method is decreased by 0.03 Hz, and the response time is shortened by 20.83%. It is clear that the optimized strategy has better power-frequency performance when the system output active set value changes.

The output current comparison between the conventional VSG dual adaptive inertia and damping control and the ANFIS-VSG dual adaptive inertia and damping control is presented in Fig. 10. Compared to the conventional method, when the islanded system connects the grid at 0.5s; the set value of active power alters at 0.6 s; and the set value of active power changes at 1.0 s; the proposed control strategy has a lesser maximum current amplitude change of 10 A, but the maximum current amplitude change of the conventional method reaches 25 A. It can be seen that the output current of the proposal control scheme can achieve the steady state more smoothly.

The variation of the rotational inertia and damping coefficients is provided in Fig. 11. It is evident that the inertia and damping regulate adaptively as the system operating conditions change at 0.2 s, 0.5 s, 0.6 s, and 1.0 s. When the system is put into load at 0.2 s, the system frequency rises, and the virtual inertia and damping coefficient of VSG generate greater adjustment relative to other time points. Additionally, the virtual inertia J and damping coefficient D have continuous smooth characteristics during the 0.5 s islanded grid operation and the 0.6 s and the 1.0 s changing the output active reference value. It can be concluded that the improved strategy enables the wind power system inverter to

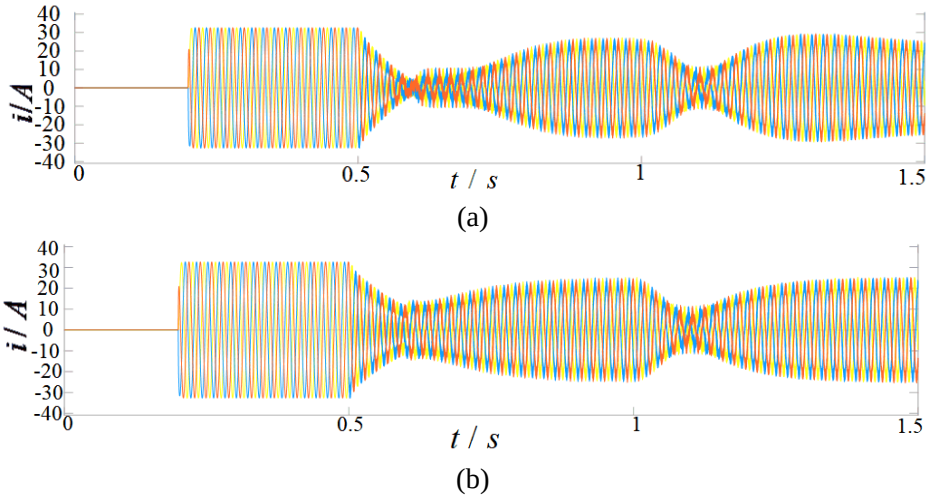

Figure 10. VSG output voltage current waveform. (a) Output three-phase current of conventional VSG dual adaptive inertia and damping control. (b) Output three-phase current of ANFIS-VSG dual adaptive inertia and damping control.

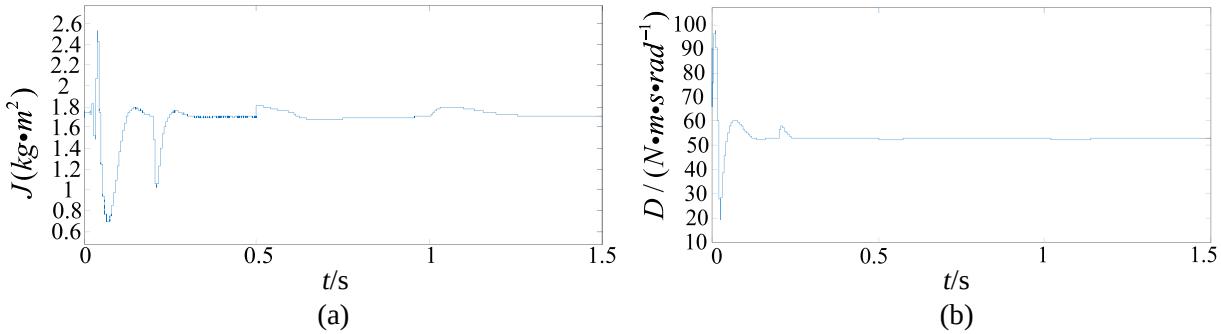

Figure 11. Trend of rotational inertia and damping coefficient during the simulation run. (a) Rotational inertia J. (b) Damping coefficient D.

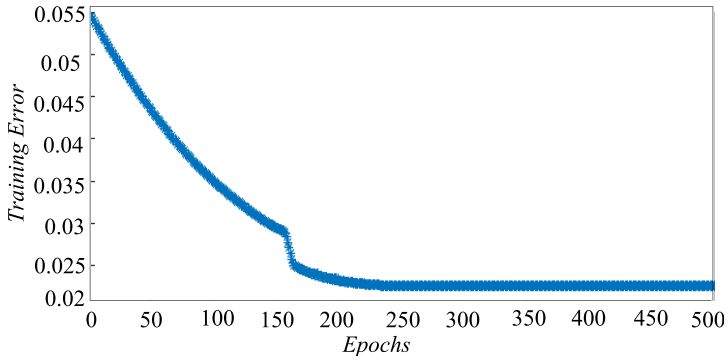

Figure 12. Training error curve.

stabilize to the target value as soon as possible during the regulation process and reduce the active overshoot.

The training error of the neural network is displayed in Fig. 12. After 500 training times, the error value has been reduced to less than 0.025°, which is an improvement of the accuracy of the ANFIS-VSG dual adaptive inertial damping control of the D-PMSWG system.

5. CONCLUSION

In this paper, the ANFIS is applied to optimize the inertia J and damping D in the VSG algorithm, so that the frequency regulation and power stabilization of the D-PMSWG system can be achieved under three operating conditions of injecting loads, connecting grid from islanded mode, and changing the active power reference value.

1) When the loads are put into the system, the optimized method restores the frequency stability sooner and limits the oscillation amplitude to a narrower range, which efficiently curbs the disturbance to the system in a brief period of time caused by the large capacity load.

2) When the system is grid-connected in islanded mode, the frequency fluctuation could be reduced and the velocity of frequency response could be expedited by the improved approach.

3) When the setting value of active power is altered, the output active power is provided with better capability to track the trajectory of the given value by the proposed method and could reach the reference value in steady state with better control accuracy, faster tracking speed, and superior frequency response performance.

In particular, the variation in the amplitude of the inverter three-phase output currents at each time node has been inhibited by the ANFIS-VSG control tactics, which supplies a more stable transition to the steady state and better immunity to disturbances. Finally, the accuracy of the proposed control algorithm has been strengthened by the training of FIS.

ACKNOWLEDGMENT

This work was supported by the National Natural Science Foundation of China under Grant Number 51907061, Educational Commission of Hunan Province of China under Grant Number 21B0552, Natural Science Foundation of Hunan Province of China under Grant Number 2022JJ50094.

REFERENCES

1. Prajapati, B. and M. C. Chudasama, "Modeling of grid connected PMSG based WECS," *2020 IEEE International Power and Renewable Energy Conference*, 1–6, Karunagappally, India, 2020, doi: 10.1109/IPRECON49514.2020.9315246.
2. Belkhier, Y. and A. Y. Achour, "Passivity-based current control strategy for PMSG wind turbine," *2019 1st International Conference on Sustainable Renewable Energy Systems and Applications (ICSRESA)*, 1–4, Tebessa, Algeria, 2019, doi: 10.1109/ICSRESA49121.2019.9182518.
3. Mi, D., T. Wang, M. Gao, and Z. Wang, "Small signal stability analysis of PMSG-VSG and optimal design for control parameters," *2020 IEEE Power & Energy Society General Meeting (PESGM)*, 1–5, Montreal, QC, Canada, 2020, doi: 10.1109/PESGM41954.2020.9282033.
4. Sun, B., Z. Chen, C. Gao, A. Haddad, J. Liang, and X. Liu, "A power decoupling control for wind power converter based on series-connected MMC and open-winding PMSG," *IEEE Transactions on Industrial Electronics*, Vol. 69, No. 8, 8091–8101, Aug. 2022, doi: 10.1109/TIE.2021.3099227.
5. Wang, T., S. Huang, M. Gao, and Z. Wang, "Adaptive extended Kalman filter based dynamic equivalent method of PMSG wind farm cluster," *IEEE Transactions on Industry Applications*, Vol. 57, No. 3, 2908–2917, May–June 2021, doi: 10.1109/TIA.2021.3055749.
6. Xu, S., S. Tao, W. Zheng, Y. Chai, M. Ma, and L. Ding, "Multiple open-circuit fault diagnosis for back-to-back converter of PMSG wind generation system based on instantaneous amplitude estimation," *IEEE Transactions on Instrumentation and Measurement*, Vol. 70, 1–13, 2021, Art no. 3512413, doi: 10.1109/TIM.2021.3062683.
7. Wu, Z., X. Zou, X. Yuan, and W. Xiong, "Review on virtual synchronous generator technologies," *The 16th IET International Conference on AC and DC Power Transmission (ACDC 2020)*, 744–751, Online Conference, 2020, doi: 10.1049/icp.2020.0253.
8. Wang, D., J. Tang, and J. Qiao, "Review of VSG for industrial process data regression modeling," *2021 40th Chinese Control Conference (CCC)*, 1316–1321, Shanghai, China, 2021, doi: 10.23919/CCC52363.2021.9549875.

9. Cheng, C., H. Yang, Z. Zeng, S. Tang, and R. Zhao, "Rotor inertia adaptive control method of virtual synchronous generator," *Power System Automation*, Vol. 39, No. 19, 82–89, 2015, doi: 10.7500/AEPS20141130003.
10. Zhu, Z., S. Huang, Z. Li, and Y. Xiao, "Research on control strategy for micro-grid adaptive rotating inertia virtual synchronous generator," *Proceedings of the CSU-EPSA*, Vol. 32, No. 4, 111–115, 2020, doi: 10.19635/j.cnki.csu-epsa.000275.
11. Li, J., B. Wen, and H. Wang, "Adaptive virtual inertia control strategy of VSG for micro-grid based on improved bang-bang control strategy," *IEEE Access*, Vol. 7, 39509–39514, 2019, doi: 10.1109/ACCESS.2019.2904943.
12. Ke, X., W. Zhang, P. Li, S. Niu, S. Sheng, and J. Yang, "Fuzzy adaptive virtual inertia control for high wind power penetration system," *Power System Technology*, Vol. 44, No. 6, 2127–2136, 2020, doi: 10.13335/j.1000-3673.pst.2019.1349.
13. Lao, H., L. Zhang, T. Zhao, and L. Zou, "Frequency regulation strategy for DFIG combining over-speed control and adaptive virtual inertia," *2019 IEEE Innovative Smart Grid Technologies — Asia (ISGT Asia)*, 1663–1666, Chengdu, China, 2019, doi: 10.1109/ISGT-Asia.2019.8881628.
14. Yue, J., X. Zhang, P. Zhou, and T. Tong, "Virtual synchronization control strategy for double-fed wind turbines based on adaptive inertia damping," *Proceedings of the CSU-EPSA*, Vol. 33, No. 9, 40–48, 2021, doi: 10.19635/j.cnki.csu-epsa.000554.
15. Li, S., W. Wang, S. Qin, X. Zhang, and C. Li, "Fuzzy adaptive virtual inertia control strategy of wind turbines based on system frequency response interval division," *Power System Technology*, Vol. 45, No. 5, 1658–1665, 2021, doi: 10.13335/j.1000-3673.pst.2020.2232.
16. Li, D., Q. Zhu, S. Lin, and X. Y. Bian, "A self-adaptive inertia and damping combination control of VSG to support frequency stability," *IEEE Transactions on Energy Conversion*, Vol. 32, No. 1, 397–398, March 2017, doi: 10.1109/TEC.2016.2623982.
17. Wang, Q., D. Zhou, S. Yin, Y. Lei, and T. He, "Improved adaptive inertia and damping coefficient control strategy of VSG based on optimal damping ratio," *2022 International Power Electronics Conference (IPEC-Himeji 2022 — ECCE Asia)*, 102–107, Himeji, Japan, 2022, doi: 10.23919/IPEC-Himeji2022-ECCE53331.2022.9806825.
18. Ban, G., Y. Xu, D. Guo, W. Zhou, H. Zheng, and X. Yuan, "Research on adaptive VSG control strategy based on inertia and damping," *2021 IEEE Sustainable Power and Energy Conference (iSPEC)*, 1584–1589, Nanjing, China, 2021, doi: 10.1109/iSPEC53008.2021.9735506.
19. Ding, J., J. Zhang, and Z. Ma, "VSG inertia and damping coefficient adaptive control," *2020 Asia Energy and Electrical Engineering Symposium (AEEES)*, 431–435, Chengdu, China, 2020, doi: 10.1109/AEEES48850.2020.9121526.
20. Gong, R. and J. Gu, "Adaptive control strategy of inertia and damping for load virtual synchronous machine," *Electrical Measurement & Instrumentation*, 1–7, 2021, doi: https://kns.cnki.net/kcms/detail/23.1202.TH.20210120.1910.014.html.
21. Li, D., Q. Zhu, Y. Cheng, Q. Liu, S. Lin, F. Yang, and X. Bian, "Control strategy of virtual synchronous generator based on adaptive inertia damping integrated control algorithm," *Electr. Power Automation Equip.*, Vol. 37, No. 11, 72–77, 2017, doi: 10.16081/j.issn.1006-6047.2017.11.012.
22. Hsu, C. F. and B. K. Lee, "FPGA-based adaptive PID control of a DC motor driver via sliding-mode approach," *Expert Systems with Applications*, Vol. 38, No. 9, 11866–11872, 2011, doi: 10.1016/j.eswa.2011.02.185.
23. Hou, B. J., J. S. Gao, X. Q. Li, et al., "Study on repetitive PID control of linear motor in wafer stage of lithography," *Procedia Engineering*, Vol. 29, No. 1, 3863–3867, 2012, doi: 10.1016/j.proeng.2012.01.585.
24. Yang, J., C. Shang, Y. Li, F. Li, L. Shen, and Q. Shen, "Constructing ANFIS with sparse data through group-based rule interpolation: An evolutionary approach," *IEEE Transactions on Fuzzy Systems*, Vol. 30, No. 4, 893–907, April 2022, doi: 10.1109/TFUZZ.2021.3049949.
25. Pournazarian, B., R. Sangrody, M. Saeedian, O. Gomis-Bellmunt, and E. Pouresmaeil, "Enhancing microgrid small-signal stability and reactive power sharing using ANFIS-tuned virtual inductances," *IEEE Access*, Vol. 9, 104915–104926, 2021, doi: 10.1109/ACCESS.2021.3100248.